P1.96

SEASONAL AND INTRASEASONAL MODULATIONS OF ENVIRONMENTAL FIELD FOR TROPICAL CYCLOGENESIS OVER THE BAY OF BENGAL

Wataru Yanase[1]*, Hiroshi Taniguchi[2] and Masaki Satoh[1,2]
1. Atmosphere and Ocean Research Institute, The University of Tokyo
2. Research Institute for Global Change, Japan Agency for Marine-Earth Science and Technology

1. Introduction

The Bay of Bengal (BoB) in the North Indian Ocean is one of the regions where tropical cyclones (TCs) are frequently formed. Although the number of tropical cyclogenesis over the BoB is less than those over the western and eastern North Pacific, TCs over the BoB have affected the human society in the surrounding countries. For example, tropical cyclone Nargis caused catastrophic destruction in Myanmar with more than 130,000 victims in 2008 (Webster 2008). The BoB is also of scientific interest, as two cyclogenesis seasons occur before and after the mature season of Asian summer monsoon (ASM): around the pre-monsoon season ($\sim$ May) and around the post-monsoon season (October $\sim$ November). Such two-peak characteristic of tropical cyclogenesis is unique to the NIO including the BoB and the Arabian Sea, whereas it is not observed over the other regions which have only a peak around summer.

Camargo et al.(2007) demonstrated that the large-scale environmental field can explain the two peaks of tropical cyclogenesis over the North Indian Ocean; they used genesis potential (GP) index proposed by Emanuel and Nolan (2004), which considers 4 environmental factors: lower-tropospheric abosolute vorticity, vertical shear, potential intensity, and mid-tropospheric relative humidity. In addition, tropical cyclogenesis over the Bay of Bengal is influenced by the boreal summer intra-seasonal oscillation (BSISO) in the Asian monsoon. Kikuchi and Wang (2010) showed that the GP was high during the active cyclogenesis phase of the BSISO. Taken together, tropical cyclogenesis over the BoB seems to become active during the high GP period caused by seasonal transition and the BSISO. Yanase et al.(2010) showed that the superposition of seasonal transition and BSISO caused the high GP responsible for the genesis of Nargis in 2008. Because their analysis mainly focused on Nargis, more statistical analysis is necessary to understand the comprehensive characteristics of the environment responsible for tropical cyclogenesis over the BoB.

In the present study, we examined the statistical relation between the tropical cyclogenesis and environmental field over the BoB by addressing the following issues: (1) What is the dominant signal of environmental field associated with the tropical cyclogenesis over the BoB? This was examined by a composite analysis of the environmental field based on cyclogenesis events. (2) Which GP factor is important for the environmental modulation caused by seasonal transition and the BSISO? (3) How much do the seasonal transition and the BSISO contribute to the total GP modulation?

2. Methodology

The large-scale environmental field analyzed in this study comprised daily data on the atmosphere and ocean between 1982 and 2008. We used atmospheric analysis data of JRA-25/JCDAS provided by the Japan Meteorological Agency (JMA) and the Central Research Instituted of Electric Power Industry (CRIEPI). The original 6-hourly dataset of JRA-25/JCDAS was averaged every four time steps to create a daily dataset. Outgoing long-wave radiation (OLR) provided by the National Oceanic and Atmospheric Administration (NOAA) was used as a proxy of convective activity. The analysis data of SST was the product of NOAA Optimum Interpolation from late 1981. The original weekly dataset of SST was linearly interpolated in time to create a daily dataset. To remove the signal of TC itself as much as possible, the environmental field was obtained by using a 15-day running mean and spatial filter.

Information regarding the locations and intensities of individual TCs was derived from a best-track dataset obtained from the International Best Track Archive for Climate Stewardship (IBTrACS) for the period 1982-2008. Here, tropical cyclogenesis was defined as the time when the surface wind speed of the best-track data reached an operational definition of a "named storm" ($\sim$ 17ms^{-1}).

The environmental field favorable for tropical cyclogenesis was examined by the GP proposed by Emanuel and Nolan (2004), which is defined based on four en-

*Corresponding author address: Wataru Yanase, Atmosphere and Ocean Research Institute, The University of Tokyo, Japan; e-mail: yanase@aori.u-tokyo.ac.jp

vironmental factors:

$$GP = |10^5\eta|^{3/2}(1+0.1V_{shear})^{-2}\left(\frac{V_{pot}}{70}\right)^3\left(\frac{H}{50}\right)^3,$$

where η is the absolute vorticity at 850 hPa (s^{-1}), V_{shear} is the magnitude of the vertical wind shear between 850 and 200 hPa (ms^{-1}), V_{pot} is the potential intensity (ms^{-1}), and H is the relative humidity (%). The potential intensity V_{pot} considers SST and vertical profiles of temperature and specific humidity in the troposphere, and is defined as

$$V_{pot}^2 = \frac{T_s}{T_0}\frac{C_k}{C_D}(CAPE^* - CAPE^b),$$

where T_S is SST, T_0 is the mean outflow temperature at the level of neutral buoyancy, C_k is the exchange coefficient for enthalpy, C_D is the drag coefficient, $CAPE^*$ is the convective available potential energy (CAPE) for an air parcel at the radius of maximum winds, and $CAPE^b$ is the CAPE for an air parcel lifted from the lowest data grid (1000 hPa) in the ambient atmosphere.

3. Results

The seasonal transition is the most important environmental modulation responsible for tropical cyclogenesis. Figure 1 shows the time-latitude diagram of basic variables averaged over the BoB (80°E-100°E). The SST is high in the pre- and the post-monsoon season, whereas it is relatively low in the mature-monsoon season (Fig. 1a). The two peaks of high SST is a unique characteristic over the BoB and the Arabian Sea in the NIO, whereas high SST in the other ocean occurs around summer season (not shown). As the tropical cyclogenesis over the BoB are also active in the pre- and post-monsoon seasons, the SST may control the cyclogenesis activity over the BoB. However, accurate seasonal and spatial distribution of the cyclogenesis activity is not explained merely by the high SST: the tropical cyclogenesis in the post-monsoon season is more active than that in the pre-monsoon season, although the SST in the post-monsoon season is lower than that in the pre-monsoon season. The convective activity, which is identified by the lowest OLR, occurs in the mature-monsoon season over the BoB (Fig. 1b). It is interesting to note that the tropical cyclogenesis over the BoB is inactive during the intense convective season, whereas those over the western and eastern North Pacific is active during summer with intense convection (not shown). Over the BoB, a monsoon flow represented by the zonal wind (Fig. 1c) changes its sign during the pre- and post-monsoon seasons. Apparently, most of the tropical cyclogenesis occurred during these transitions of the monsoon flow. Meridional temperature gradient (MTG) in the upper troposphere (200–500 hPa) is another index of the ASM. Whereas the MTG is generally negative in the northern hemisphere due to the meridional difference of solar radiation, the MTG during the mature ASM is uniquely positive due to the heating of the Asian continent to the north of the BoB. Again, most of the tropical cyclogenesis over the BoB occurred during the pre- and post-monsoon season when the MTG changes its sign (Fig. 1d).

In order to understand why the pre- and post-monsoon season is favorable for tropical cyclogenesis, the seasonal transition of climatological GP and its four factors are shown in Fig. 2. There are two peaks of high GP in pre- and post-monsoon season (Fig. 2a), which is in good agreement with the TC activity over the BoB. The relation between the GP and tropical cyclogenesis is consistent with the result of Camargo et al.(2007). In addition, the high GP appears to explain the latitudes of tropical cyclogenesis qualitatively including a northward shift in the pre-monsoon season and a southward shift in the post-monsoon season. Note that tropical cyclogenesis in the southern hemisphere also occurs during the high GP seasons, which occur from October to May. The four GP factors give detailed information on the environmental field favorable for tropical cyclogenesis. The seasonal transition of absolute vorticity is relatively weak due to the dominance of meridional gradient of planetary vorticity (Fig. 2b). Apparently, weak vertical shear in the pre- and post-monsoon seasons are in good agreement with the two peaks of high GP over the BoB (Fig. 2c). Based on the thermal wind balance, the weak vertical shear is associated with the small MTG in pre- and post-monsoon seasons over the BoB (Fig. 1d). The potential intensity is high in pre- and post-monsoon seasons (Fig. 2d), which also contribute to the two peaks of high GP over the BoB. The high potential intensity is attributed to the high SST in the BoB as shown in Fig. 1a. On the other hand, the mid-tropospheric relative humidity is largest during the mature-monsoon season (Fig. 2e), which is related to the active convection as shown in Fig. 1b. Thus, in the climatological field, the high GP in the pre- and post- monsoon seasons over the BoB is attributed to the weak vertical shear and high potential intensity.

If the large-scale environmental field modulates in the time-scale shorter than the seasonal transition, it is of interest to examine whether individual tropical cyclogenesis occurred during the high GP period of the modulation. To extract signals of the modulation of environmental field, a composite analysis based on cyclogenesis event is attempted (TC-based composite analysis), in which environmental fields were averaged for all the tropical cyclogenesis days. In addition, the composite was also performed for days before and after the cyclogenesis (referred to as relative days), which provides the time scale of the large-scale modulation. Two sets of data were prepared for the TC-based composite analysis: one is the data of individual year in which a cyclogenesis occurred (total field), and the other is the data of climatology between 1982 and 2008 (climatological field). In addition, by subtracting the climatological field from the total field, the anomaly field is obtained. As the cyclogenesis activity and climatological fields are different between seasons (Figs. 1 and 2), a year was separated into three seasons: April-May (AM; pre-monsoon over the BoB), June-July-August September (JJAS; mature-monsoon) and October-November (ON; post-monsoon).

Figure 3 shows the time-latitude diagram of the TC-composite field for GP. Here, the relative day 0 is the time when cyclogenesis occurred (short horizontal bars in Fig. 3). In the pre-monsoon season (the left column in Fig. 3), a high GP signal in the total field shifted northward from -20 day to 10 day (Fig. 3a). The climatological field contributed to the high GP in the total field (Fig. 3d), and slowly shifted northward, which is a seasonal transition observed in Fig. 2a. However, the climatological field is not sufficient to explain the fast northward shift of high GP signal in the total field. The anomaly field shows fast northward shift of positive GP anomaly, from -20 day to 10 day (Fig. 3g), which apparently contributes to the total field. The fast northward shift of high GP has a periodicity of $\sim$ 40 days. Most of the tropical cyclogenesis occurred in this positive GP anomaly. In the mature-monsoon season (the middle column in Fig. 3), the fast northward signal of high GP in the anomaly field was also observed, whereas the climatological field is stationary with high GP between 10°N and 20°N. In the post-monsoon season (the right column in Fig. 3), a weak northward shift of high GP in the anomaly field still occurred, even though the climatological field shows slow southward shift of the high GP region. Thus, the northward shift of high GP region with the intra-seasonal timescale ($\sim$ 40 days) occurred in all the seasons, although the signal is weak in the post-monsoon season.

The detailed results of TC-basec composite analysis (not shown) is summarized as follows: the tropical cyclogenesis in the pre-, mature-, and post-monsoon seasons occurred within the northward moving signal of the high GP anomaly, which had a horizontal scale more than 50° and the periodicity of $\sim$ 40 days. The high GP is attributed to the large absolute vorticity and high relative humidity in all the seasons, whereas it is also attributed to the weak vertical shear in the mature-monsoon season; The tropical cyclogenesis in the mature-monsoon season occurred slightly to the north relative to the phase of northward moving signals compared to the pre- and post-monsoon seasons. The signal was more significant in the pre- and mature-monsoon seasons than in the post-monsoon season. The significant signal in the TC-based composite indicates that there is a dominant dynamics which controls the tropical cyclogenesis environment over the BoB.

As the modulation of GP seems to be related to the BSISO, the relation between tropical cyclogenesis and BSISO was examined. Based on the previous studies, the BSISO was defined by the 30-60-day filtered zonal wind at 850 hPa in boreal summer. Here, the data for summer season is months from May to October because the MTG over the BoB is almost positive (Fig. 1d), and because the amplitude of the BSISO mode is large Kikuchi and Wang (2010). To remove the influence of the TC itself on the BSISO signal, the zonal flow is averaged in the area of 60°E–110°E and 10°N–20°N (rectangle in Fig. 4), which is determined based on the structure of the BSISO shown in the previous studies. Each minimum-maximum-minimum cycle is divided into eight phases in the following manner: Phases 1–4 (5–8) is defined by separating the period from the first minimum to the maximum (from the maximum to the second minimum) evenly. The composite of large-scale fields and the count of cyclogenesis were performed based on the phases of the BSISO.

Figure 4 shows the horizontal pattern of zonal wind at 850 hPa and OLR for Phases 1, 3, 5 and 7. In Phase 1, westerly anomaly is observed near the equator over the Indian Ocean, and active convection (negative OLR) occurs to the north of the westerly maximum. From Phase 1 to Phase 5, the westerly anomaly and active convection shifted northward from the equator to the BoB. In Phase 7, the westerly anomaly almost disappeared over the Indian Ocean, which is the end of the BSISO cycle. Figure 5a shows the number of tropical cyclogenesis for each phase. Tropical cyclogenesis is significantly modulated by the phase of BSISO: the number of tropical cyclogenesis in Phases 3 and 4 is more than 10, whereas those in Phases 1, 6, 7 and 8 is less than 2. Phases

3 and 4 is characterized by active convection over the BoB (Fig. 4). This is consistent with the result of Kikuchi and Wang (2010) which identified the BSISO by an extended empirical orthogonal function (EEOF). Figure 5b confirms that the analyzed days of each phase are almost the same (about 600 days). Therefore, the modulation of the cyclogenesis number between phases should be attributed to the difference of some dynamics, rather than to the difference of sample number of analyzed days.

The phase-latitude diagrams of GP and its four factors in the BSISO-based composite analysis are shown in Fig. 6, together with individual tropical cyclogenesis. The total GP shows a maximum around Phase 3 between 15°N and 20°N, where tropical cyclogenesis is active (Fig. 6a). The anomaly field of GP shows a positive signal moving northward from Phase1 to Phase 4 (Fig. 6a). The tropical cyclogenesis is active around the maximum of positive GP anomaly, although the timing seems to be a little delayed. To estimate the contribution of each GP factor to the total GP quantitatively, the GP was recalculated using the environmental field of individual cases for one factor and the field of the climatology for the other three factors. Figure 6c–6f shows the contribution of the four factors to the GP anomaly, whose magnitude can be directly compared with each other. As seen in the TC-based composite in Section 4, the absolute vorticity and relative humidity seem to contribute the modulation of tropical cyclogenesis. Furthermore, this quantitative analysis shows that the relative humidity contribute to the GP modulation more significantly than the absolute vorticity. It should be also noted that the vertical shear seems to contribute to the tropical cyclogenesis from June to September (Fig 6d).

4. Summary

The environmental field responsible for tropical cyclogenesis over the BoB was examined from the pre-monsoon to post-monsoon seasons using the TC best-track data and atmosphere/ocean analysis data. The GP index and its four factors Emanuel and Nolan (2004) were applied to the seasonal and intra-seasonal environmental modulations.

In the climatological field, the two peaks of tropical cyclogenesis activity was unique to the NIO including the BoB and the Arabian Sea (not shown). This was attributed to the high GP during the pre- and post-monsoon seasons over the NIO, which is consistent with previous works (Camargo et al. 2007; Kikuchi and Wang 2010). In addition, the analysis of four GP factors demonstrated that the weak vertical shear and high potential intensity contributed to the two peaks of GP over the BoB.

The TC-based composite analysis extracted the northward moving signal of high GP, which is also unique to the NIO in summer season. The signal of high GP was enough large to modulate the total GP field. As the signal had zonal-scale more than 50° and the periodicity of $\sim$ 40 days, it is attributed to the BSISO in the ASM. The BSISO-based composite analysis showed that tropical cyclogenesis is active within the high GP phase of the BSISO. The high GP phase was associated with the high relative humidity and large absolute vorticity in the convective phase of the BSISO. During the mature-monsoon season, the phase with weak vertical shear in the BSISO also seems to contribute to the high GP, probably because the strong vertical shear in the climatological field strongly inhibit the tropical cyclogenesis over the BoB.

Acknowledgement

We acknowledge helpful comments by Dr. Tetsuo Nakazawa, Dr. Yukari Takayabu, Dr. Hatsuki Fujinami, Dr. Satoru Yokoi and Dr. S. J. Camargo. This research was supported by Core Research for Evolutional Science and Technology, Japan Science and Technology Agency (CREST, JST) and KAKENHI 20740266.

References

Camargo, S. J., K. A. Emanuel, and A. H. Sobel, 2007: Use of a genesis potential index to diagnose ENSO effects on tropical cyclone genesis. J. Clim., 20, 4819—4834.

Camargo, S. J., M. C. Wheeler, and A. H. Sobel, 2009: Diagnosis of the MJO modulation of tropical cyclogenesis using an empirical index. J. Atmos. Sci., 66, 3061—3074.

Emanuel, K. A. and D. S. Nolan, 2004: Tropical cyclone activity and global climate. Proc. of 26th Conference on Hurricanes and Tropical Meteorology, American Meteorological Society, Miami, FL., 240—241.

Kikuchi, K. and B. Wang, 2010: Formation of Nargis (2008) and tropical cyclones in the Northern Indian Ocean associated with with tropical intraseasonal oscillation. J. Meteorol. Soc. Japan, in press.

Yanase, W., H. Taniguchi, and M. Satoh, 2010: The genesis of tropical cyclone nargis (2008): environmental modulation and numerical predictability. J. Meteorol. Soc. Japan, in press.

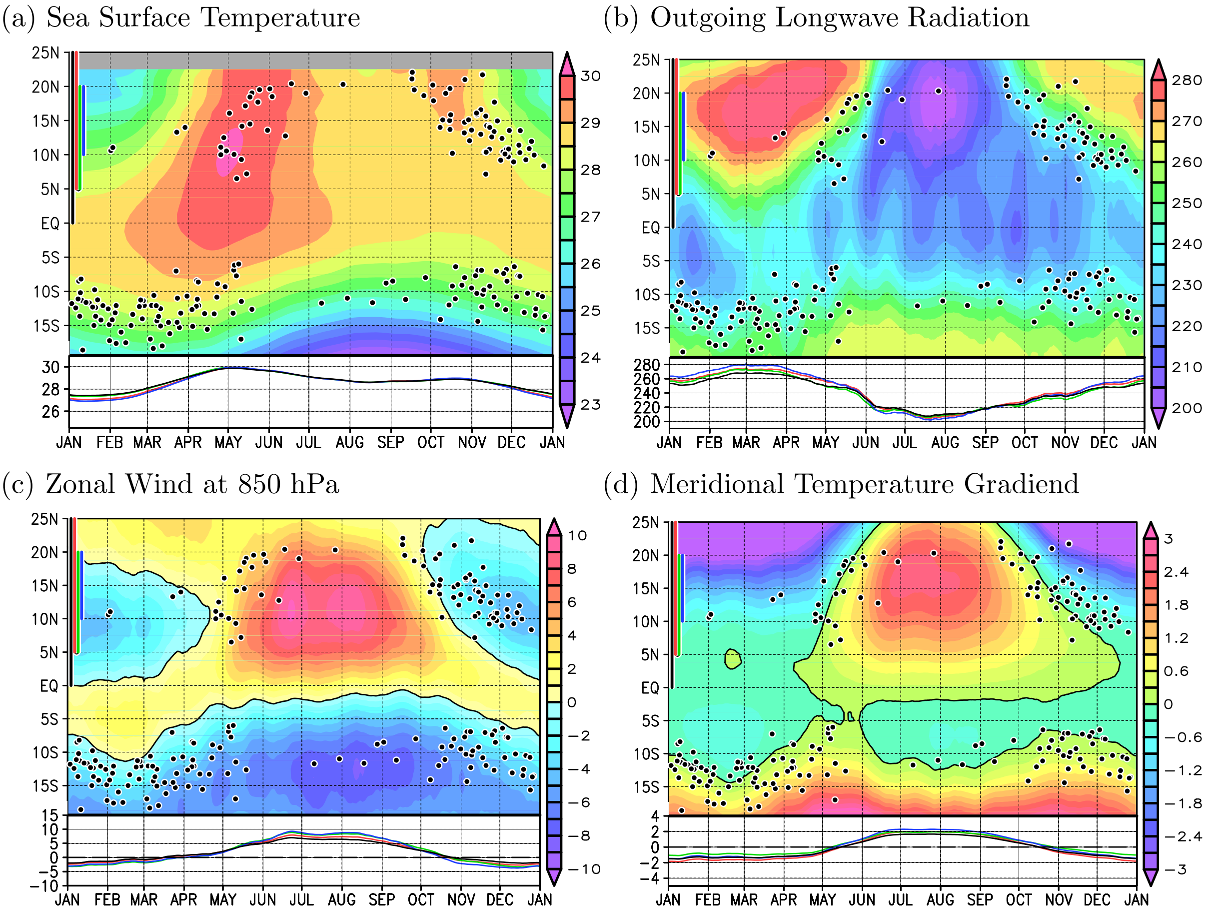

Figure 1: Time-latitude diagram of climatological basic variables averaged over the BoB (80°-100°E). (a) SST (°C); (b) OLR (Wm^{-2}) (c) zonal wind at 850 hPa (ms^{-1}); (d) MTG ($10^{-6}Km^{-1}$). Black, red, green and blue curves at the bottom of the panels show the averages in 0°-25°N, 5°-25°N, 5°-20°N and 10°-20°N, respectively (the ranges are shown at the top-left of the panels). Black circles indicate the time and latitude of tropical cyclogenesis.

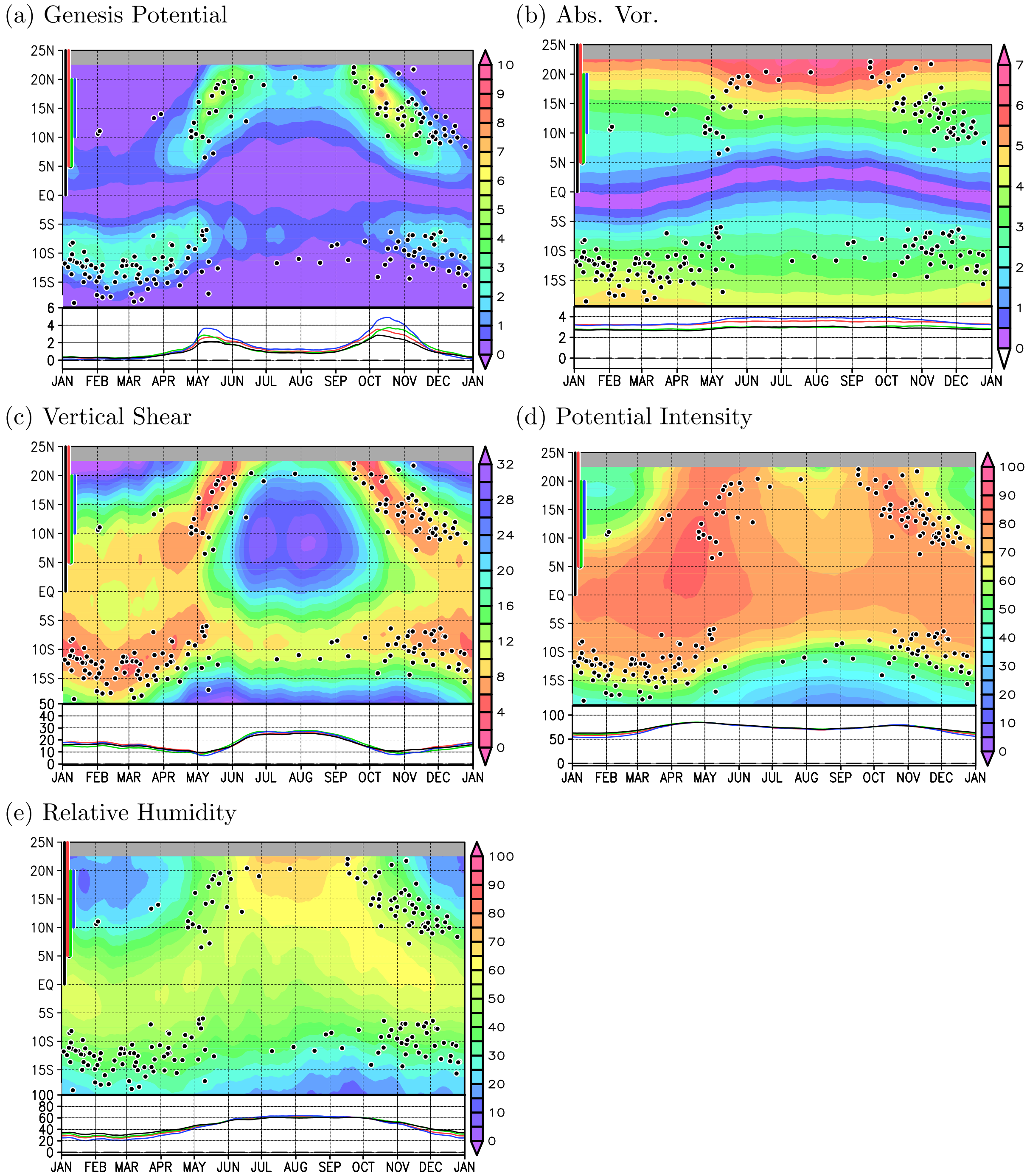

Figure 2: As for Fig. 1, but for (a) GP; (b) absolute vorticity ($10^5\mathrm{s}^{-1}$); (c) vertical shear between 850 and 200 hPa (ms^{-1} / 650 hPa); (d) potential intensity (ms^{-1}); and (e) relative humidity at 600 hPa.

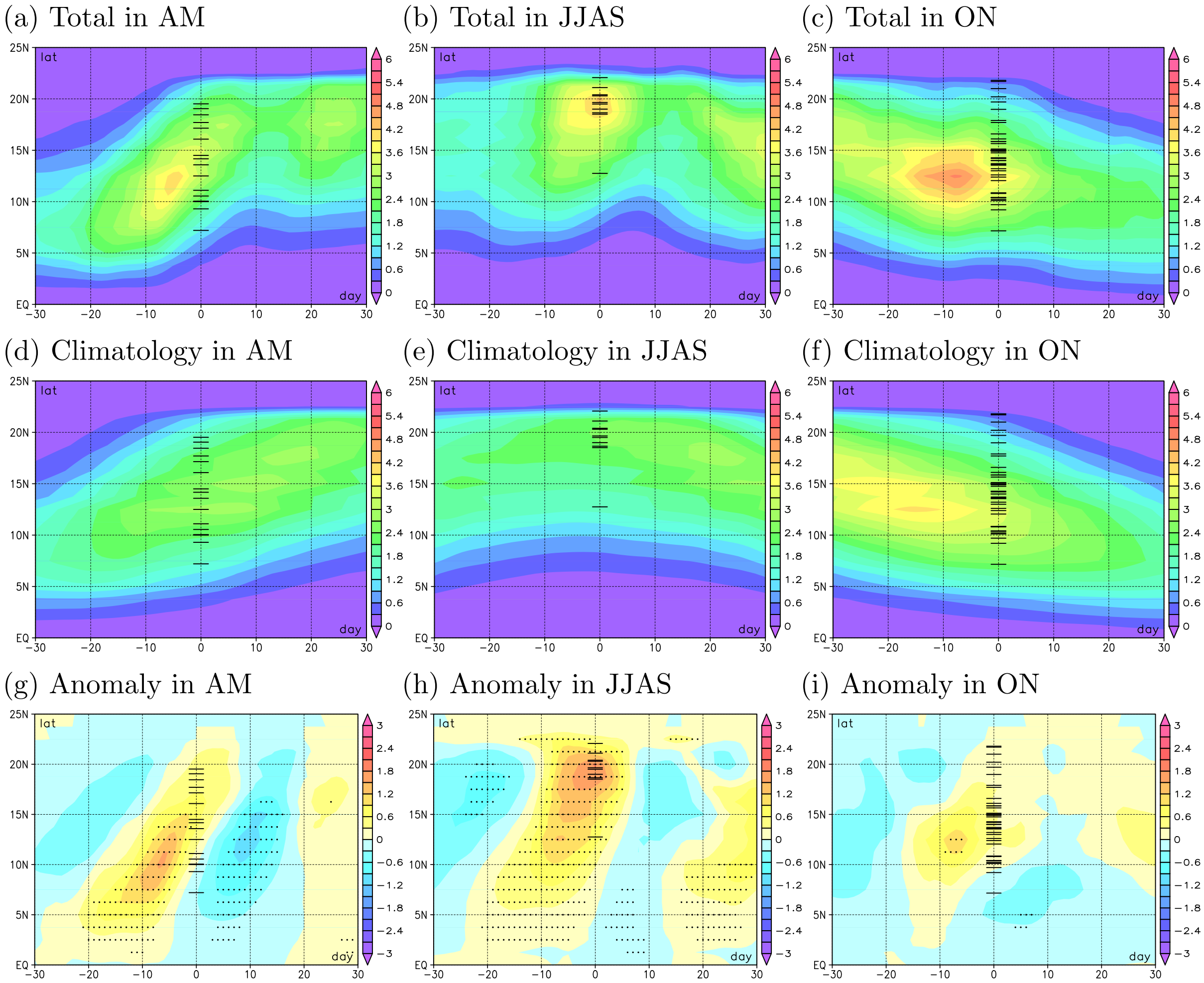

Figure 3: Time-latitude diagram of GP over the BoB in the TC-based composite analysis. Left (a, d and g), middle (b, e and h), and right (c, f and i) panels for months of AM, JJAS, and ON, respectively. Top (a, b and c), middle (d, e and f), and bottom (g, h and i) panels for total, climatology, and anomaly, respectively. Dotted areas correspond to differences in the anomaly at $p \prec 0.05$ using Student's t-test. Short horizontal bars at day 0 indicate the latitudes of individual cyclogenesis.

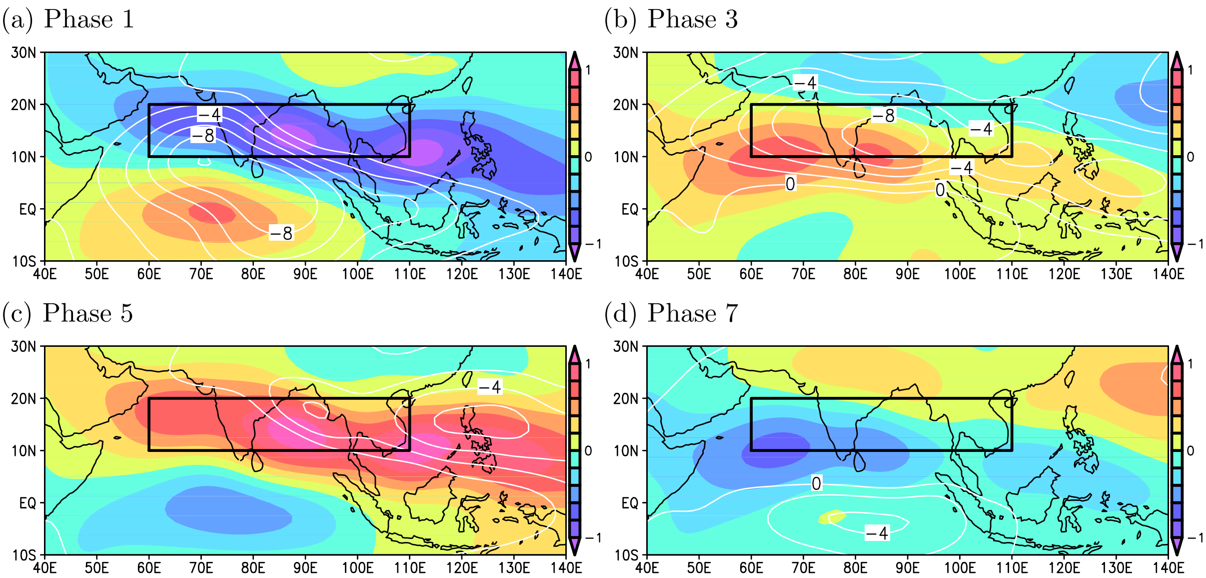

Figure 4: Composite of zonal wind anomaly at 850 hPa (shade) and negative OLR anomaly (white contours with contour interval of 2 Wm^{-2}) for (a) phase 1, (b) phase 3, (c) phase 5, and (d) phase 7 of BSISO. The black rectangle shows the region in which the index of zonal wind was averaged.

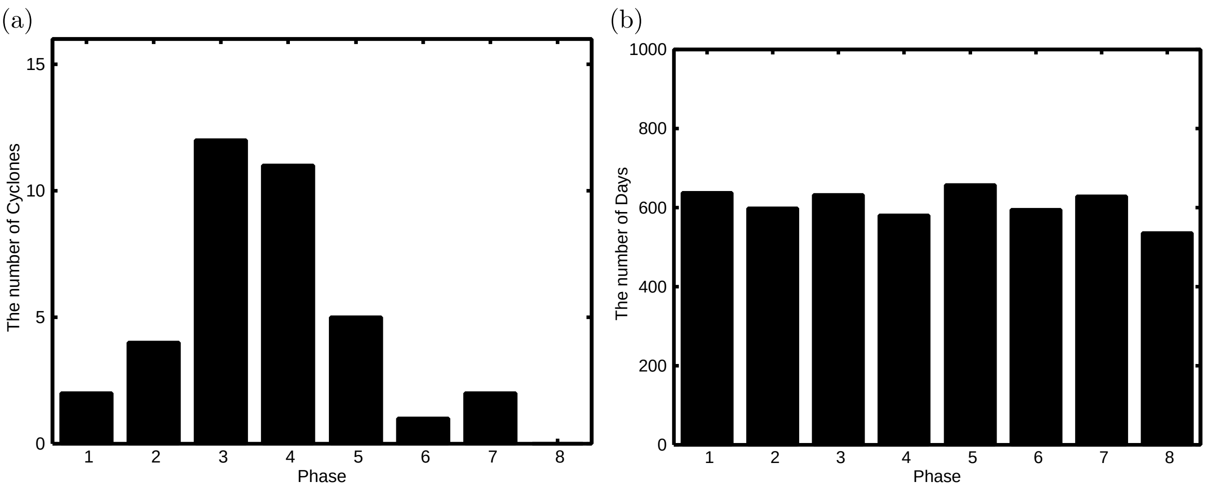

Figure 5: Numbers of the events in each phase of the BSISO. (a) Tropical cyclogenesis. (b) Total observed day.

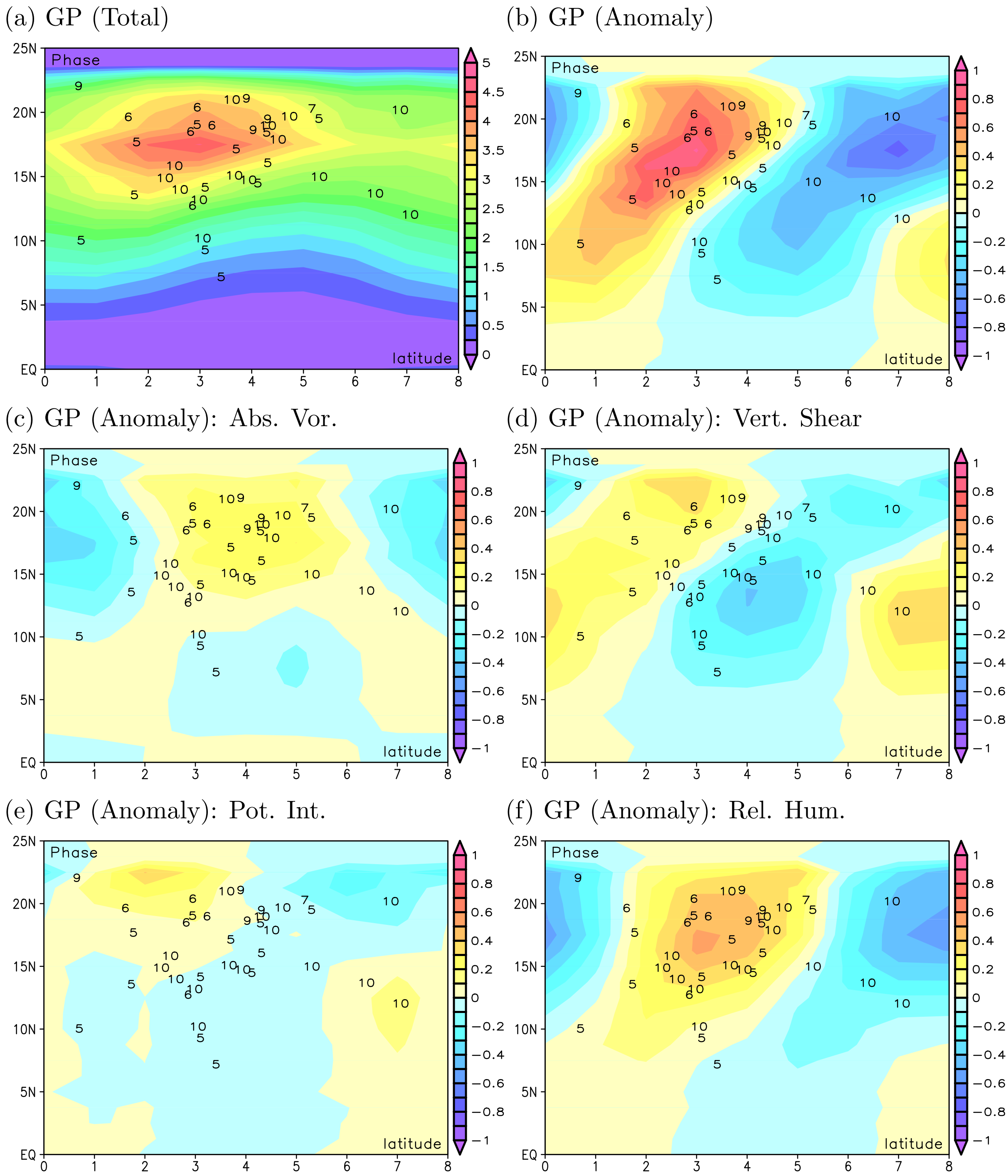

Figure 6: Phase-latitude diagram obtained by the BSISO-based composite analysis. (a) GP (total); (b) GP (anomaly); (c) contribution of absolute vorticity to GP (anomaly); (e) contribution of vertical shear to GP (anomaly); (f) contribution of potential intensity to GP (anomaly); (g) contribution of relative humidity to GP (anomaly). The phases, latitudes, and months of individual tropical cyclogenesis are indicated by the horizontal axis, vertical axis and values of the digits in the diagram, respectively.